ELSEVIER

Earth and Planetary Science Letters 181 (2000) 251–264

EPSL

www.elsevier.com/locate/epsl

Bubble growth in rhyolitic melt

Yang Liu, Youxue Zhang *

The Department of Geological Sciences, The University of Michigan, Ann Arbor, MI 48109-1063, USA

Received 27 October 1999; received in revised form 5 June 2000; accepted 8 June 2000

Abstract

We report experimental data of bubble growth in natural rhyolitic melt with 1.4–2.0 wt% initial total H_2O at 0.1 MPa and 500–600°C. Growth of many bubbles is monitored in every experiment. Bubble growth rate increases with temperature and initial total H_2O. At a given temperature and initial total H_2O, bubble growth rate also increases slightly with bubble size. The average growth rate for bubbles growing in an infinite rhyolitic melt at a bubble radius of 25 μm is $\sim$0.038 μm/s at 600°C and 2.0 wt% $H_2O_{t,i}$, $\sim$0.0064 μm/s at 550°C and 2.0 wt% $H_2O_{t,i}$, $\sim$0.00034 μm/s at 500°C and 2.0 wt% $H_2O_{t,i}$, and $\sim$0.007 μm/s at 600°C and 1.45 wt% $H_2O_{t,i}$. Our data show that bubble growth is controlled by both viscous flow and diffusion, with viscous flow playing a dominant role at the initial stage. We used the numerical bubble growth model of Proussevitch and Sahagian [J. Geophys. Res. 103 (1998) 18223–18251] to calculate bubble growth rate. Using recently assessed solubility, diffusivity, and viscosity models, the bubble growth model can reproduce our experimental data to within a factor of about 2. Adjusting the viscosity model by a factor of up to 5 (within the stated 2σ uncertainty of a factor of 8.3) generates almost perfect fits to our data. (Adjusting other parameters within uncertainty does not help significantly.) Other recent bubble growth data, except those at 0.1 MPa and 375–460°C with 5.0 wt% initial H_2O, are also consistent with the calculation. This is the first experimental verification of a bubble growth model in a silicate melt. We suggest that the verified model can be applied with confidence to quantify bubble growth during volcanic eruptions.

Keywords: bubbles; growth rates; eruptions; viscosity

1. Introduction

Bubble growth is a key process in gas-driven volcanic eruptions. There have been both experimental studies of bubble growth in natural silicate melts and numerical investigations to understand bubble growth in volcanic systems. Murase and McBirney [1] were the first to experimentally investigate bubble growth rate and nucleation in a natural rhyolitic obsidian with $\sim$0.2 wt% initial total H_2O (referred to as $H_2O_{t,i}$ hereafter) at 0.1 MPa and 800–1100°C. Bagdassarov et al. [2] studied bubble growth in a peralkaline rhyolitic melt containing $\sim$0.14 wt% $H_2O_{t,i}$ at 0.1 MPa and 625–925°C using a video camera. Lyakhovsky et al. [3] examined bubble growth at 15–145 MPa and 780–850°C using the data from bubble nucleation experiments by Hurwitz and Navon [4]. Navon et al. [5] conducted bubble growth experiments using experimentally hydrated slabs of rhyolitic glass with 5 wt% $H_2O_{t,i}$ at 0.1 MPa and

* Corresponding author. Tel.: +1-734-763-0947; Fax: +1-734-763-4690; E-mail: youxue@umich.edu

0012-821X/00/$ – see front matter
PII: S0012-821X(00)00197-7

375–460°C. Gardner et al. [6] investigated bubble growth under constant-rate decompression.

In addition to the experimental studies, many bubble growth models (e.g., [3,5,7–13]) have been developed. The models are becoming increasingly sophisticated, progressing from growth of a single bubble in an infinite liquid to growth of multiple bubbles, from constant temperature and pressure to variable temperature and pressure, and from assuming H_2O-independent diffusivity and viscosity to incorporating the dependence on H_2O. Sparks [8] developed a numerical model for bubble growth in an infinite melt. Toramaru [9,10] modeled homogeneous nucleation and subsequent bubble growth with assumptions of constant diffusivity and viscosity. In three papers [11–13], Proussevitch and coworkers investigated diffusive growth of closely spaced bubbles with a finite spherical melt shell surrounding each bubble. Incorporating H_2O-dependent viscosity and diffusivity, they numerically solved a system of equations involving mass and momentum conservation. In an effort to find a simpler model of bubble growth, Lyakhovsky et al. [3] proposed a quasi-static model for bubble growth at the initial stage (in an infinite melt with constant viscosity). Navon et al. [5] continued the approach of Lyakhovsky et al. [3] by allowing the viscosity and diffusivity to vary and tried to experimentally verify the bubble growth model.

Verification of a bubble growth model is critical for its application in volcanology. The purpose of this study is to provide high-quality and well-documented experimental data of bubble growth to verify bubble growth models. Because the data in [1,2] can be used to test models at low total H_2O (0.14–0.2 wt%, referred to as H_2O_t hereafter), those in [3,5] can be used to test models at high H_2O_t ($\sim$5 wt%), and those in [6] can be used to test models with constant-rate decompression, we report experimental data in the intermediate H_2O_t range (1.3–2.0 wt%). Because critical input expressions for melt viscosity [14], H_2O diffusivity [15–18] and solubility [16] are available, it is now possible to verify the applicability of bubble growth models. The differences between this and previous investigations of bubble growth also include: (i) we document in detail the initial and boundary conditions for the growth of each bubble and (ii) we evaluate experimental uncertainties by measuring growth data of many bubbles simultaneously in a single sample.

2. Experimental and analytical methods

2.1. Analyses of H_2O_t and CO_2

Water contents of samples before and after experiments were analyzed with a Nicolet 60SX Fourier transform infrared spectrometer. The sample chamber is purged with dry N_2. A few points in a sample were analyzed in a region without bubbles before the experiments. Similar measurements were made in the sample (far away from edges) after the experiments. More points were analyzed for less homogeneous samples. Water concentrations were calculated using the calibration of Zhang et al. [19]. Measurement precision for total H_2O concentration is 1% relative. However, measured total H_2O concentration in a sample can vary more than this due to sample heterogeneity.

Dissolved CO_2 contents of samples before the experiments were estimated from the 2350 cm^{-1} band of the same spectra obtained for H_2O determination. The precision is 5–10% relative because the NIR source–beamsplitter–detector combination is not optimized for this wavenumber region. The CO_2 concentration was determined using the extinction coefficient of 94.5 l mol^{-1} mm^{-1} [20]. The CO_2 contribution of air was examined and found to be negligible ($<1\%$ of CO_2 band intensity) by ratioing background spectra measured at different times of the same day to each other.

2.2. Sample preparation and characterization

Experiments were performed on natural obsidian glasses from the Mono Craters (site bb [21]). Samples that are free of crystals and contain only a limited number of bubbles (10–20) are most appropriate for our bubble growth experiments. Over 100 doubly polished obsidian chips were examined, and only three pieces were found to be suitable for bubble growth experiments: one

with 1.97–2.04 wt% $H_2O_{t,i}$ (the sample is referred to as sample B1 hereafter), one with 1.3–1.5 wt% $H_2O_{t,i}$ (referred to as sample B2 hereafter) and one with 1.4–1.5% $H_2O_{t,i}$ (referred to as sample B3 hereafter). Among these, sample B1 is the best due to the smaller number of bubbles and the homogeneity in H_2O_t. The samples also contain some dissolved CO_2, $\sim$36 ppm for sample B1, $\sim$21 ppm for B2 and $\sim$15 ppm for B3. These concentrations are in agreement with those in [22].

Roughly cubic pieces with sides of 1–2 mm were cut from those samples. Bubbles chosen to be studied in each small piece were numbered. Bubble sizes and positions (in *X-Y-Z* coordinates) were measured using a microscope. The distance between bubbles and between a bubble and its nearest surface was calculated. The error in the determination of the bubble diameter is typically $\sim$1 μm, but can be as large as 5 μm for bubbles with a blurred edge. The error in *X* and *Y* determination is usually $\pm$11 μm. The relative error in determining *Z* is about 10%. For samples of irregular shape (B1-3, B1-5 and B3-1), the error in the distance determination between a bubble and a slanted surface may be as large as 100 μm. More detailed information on sample characterization can be found in the **EPSL Online Background Dataset**[1].

2.3. Bubble growth experiments

We used the heat-and-quench technique (heat and hold the sample at a constant temperature for a prescribed period, quench, then measure bubble sizes by a microscope, and then heat and hold the sample to the same temperature to repeat the sequence) for bubble growth experiments to monitor the growth of many bubbles in a single sample. One disadvantage of the heat-and-quench technique is that it cannot quantify rapid bubble growth. Another disadvantage is the effect of quench on bubble size because the measurement is made at room temperature. Bubble shrinkage during quench was evaluated from stress distribution around an inclusion [23] and is about 0.4% relative for bubble diameter (depending on temperature). Because all bubble diameter data were measured at room temperature and because 0.4% relative error is tolerable, the data are internally consistent and the 0.4% correction was not made.

Heating experiments were conducted in two horizontal tube furnaces at atmospheric pressure. The sample was wrapped in a piece of aluminum foil, and placed in the hot spot adjacent to either a type S or a type K thermocouple. The temperature gradient in the silica tube was <1°C within 5 mm of the hot spot for both furnaces. Temperature became stable in less than 1 min. The samples were heated for many periods at the same temperature, each with a duration of 5–199 min. At the end of each heating period, the sample was quenched in air or liquid nitrogen, and the diameters of bubbles were measured. The repeated heating steps for a given sample at the same temperature will be referred to as a series of experiments.

3. Results

Five series of bubble growth experiments were conducted using pieces of B1 (1.97–2.04 wt% $H_2O_{t,i}$) at 500–600°C, two series using B2 (1.3–1.5 wt% $H_2O_{t,i}$) at 575–600°C, and one series using B3 (1.4–1.5 wt% $H_2O_{t,i}$) at 600°C (Fig. 1). A summary of experimental conditions for selected bubbles is shown in Table 1, and the complete bubble growth data can be found in the **EPSL Online Background Dataset**[1] (table A1). There are some complexities in the data, including: (i) appearance of new bubbles, which are monitored, (ii) the effect of diffusive loss of H_2O_t from a surface on the growth of bubbles close to that surface, (iii) the effect of diffusive loss of H_2O_t to a bubble on the growth of its closest neighboring bubble, (iv) heterogeneity in $H_2O_{t,i}$, (v) role of dissolved CO_2 in increasing pressure in the bubble [24] and bubble growth rate. These complexities are discussed in detail in **EPSL Online Background Dataset**[1]. Complexities (ii) and (iv) are significant, and the subsequent discussion takes these complexities into account. Owing to all these

[1] http://www.elsevier.nl/locate/epsl; mirror site: http://www.elsevier.com/locate/epsl

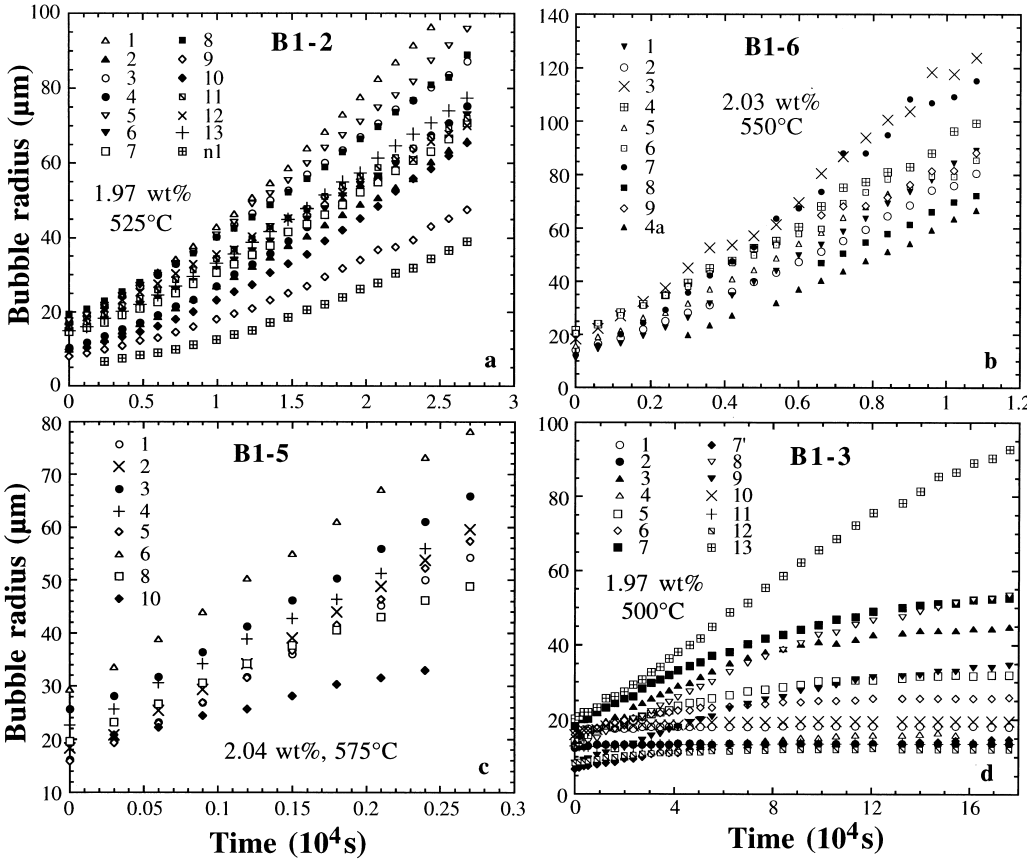

Fig. 1. Growth data for some bubbles in four series of experiments. Numbers in the legend indicate bubble number. Sample name, experimental temperature and $H_2O_{t,i}$ content are shown in each figure. The experimental pressure is 0.1 MPa.

complexities, our best data are for samples B1-2 (525°C, 1.97 wt% $H_2O_{t,i}$) and B1-6 (550°C, 2.03 wt% $H_2O_{t,i}$) because they are relatively homogeneous in H_2O_t and because they initially contain only a limited number of bubbles.

3.1. Bubble nucleation and coalescence

New bubbles appeared during bubble growth experiments either by growth of submicrometer bubbles which were initially undetected or by new nucleation. Some new bubbles appear on or near a microlite or microphenocryst, or inside microlite-rich bands. Hence, bubble appearance/nucleation in our experiments is heterogeneous. The number of new bubbles in an experiment depends on the initial presence of microlites and microphenocrysts, the temperature of the experiment, and H_2O_t content. Growth data of new bubbles were also recorded when the new bubbles were easily identifiable and not in concentrated bubble bands.

Coalescence or near-coalescence of bubble pairs has been observed in most samples (Fig. 2). Spherical walls of both bubbles are first flattened, and the melt region between them is thinned due to the growth of both bubbles (Fig. 2a). Then, the larger bubble becomes more concave, the smaller bubble becomes more convex into the larger bubble (Fig. 2b), and the melt region between the two bubbles becomes thinner and thinner. Finally the wall between two bubbles ruptures and two bubbles merge into an ellipsoidal bubble (which was observed in B2-C), which gradually relaxes to a spherical bubble (as observed in B3-1). Coales-

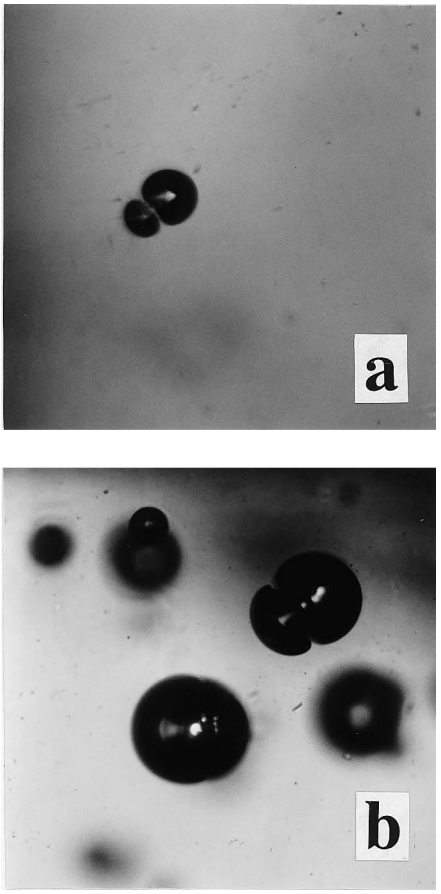

Fig. 2. Near coalescence of bubbles in sample B2-1. (a) A pair of bubbles grew close to each other. Walls of bubbles near the contact were flattened, and melt between bubbles was thinned (200×). (b) Two pairs of bubbles near the beginning of coalescence (100×).

cence of many bubbles has also been observed. In sample B2-C, a corner initially containing many bubbles became a foam, and fractures formed on the nearest surface.

3.2. Bubble growth data

The growth for each bubble follows a smooth curve (Fig. 1). Most bubbles shown in Fig. 1a–c are unaffected by surfaces or other bubbles (i.e., bubbles growing in an infinite liquid; hereafter these bubbles are referred to as unaffected bubbles for simplicity). Their growth rates increase with time and the growth curves deviate from the square-root relation between radius and time, indicating that besides diffusion, viscous flow also plays an important role. The growth at the initial stage is somewhat exponential (viscosity-controlled), consistent with the results of [5]. However, the whole growth curve cannot be simplified as either diffusion-controlled (meaning low viscosity), or viscosity-controlled (rapid diffusion), or simply viscous (no mass transport) growth. For bubbles close to a surface (e.g., bubbles 1, 2, and 11 in Fig. 1d), the growth curve may not increase as rapidly as that of unaffected bubbles, or may become flat with time.

In a given series of experiments, the growth curves for all unaffected bubbles have a similar shape. Bubbles with similar initial sizes follow similar growth curves (e.g., bubbles 1, 3, 5, and 8, and bubbles 10 and 13 in Fig. 1a), demonstrating the reproducibility of bubble growth data to be within 20% relative. Furthermore, it is likely that much of the 20% difference is attributable to local heterogeneity in $H_2O_{t,i}$. As shown later, a 13% relative variation in $H_2O_{t,i}$ can cause a factor of 2.2 variation in bubble growth rate, meaning a 3% relative variation in $H_2O_{t,i}$ (such as 1.98–2.04 wt%) is enough to cause 20% variation in bubble growth rate. Fig. 1 also shows that bubbles with larger initial size grew slightly more rapidly. The growth curves of unaffected bubbles with different initial sizes can be slid along the horizontal (time) axis so that they roughly overlap. Such overlap demonstrates consistency and means that growth rates for bubbles of different initial sizes are similar at a fixed radius (such as 25 μm) although they reach this radius at different times. The greater growth rate for larger bubbles will be explained later.

When bubble growth rates in different series of experiments are compared, bubbles grow faster at higher temperature and in melt with higher $H_2O_{t,i}$, as expected. The average growth rate for unaffected bubbles at a bubble radius of 25 μm is ~0.038 μm/s (0.033–0.042 μm/s) at 600°C and 2.0 wt% $H_2O_{t,i}$, ~0.0135 μm/s at 575°C and 2.0 wt% $H_2O_{t,i}$, ~0.0064 μm/s (0.0054–0.0082 μm/s) at 550°C and 2.0 wt% $H_2O_{t,i}$, ~0.0021 μm/s (0.0018–0.0025 μm/s) at 525°C and 2.0 wt% $H_2O_{t,i}$, 0.00034 μm/s at 500°C and 2.0 wt%

Table 1
Experimental conditions for selected bubbles

	Initial radius (μm)	Closest surface[a] (CS)	Distance to CS[b] (mm)	Closest bubble (CB)	Distance to CB[b] (mm)	S_0 (mm)	Total time (s)	t_d^c (s)
B1-1 ($H_2O_{t,i}$ = 2.03 wt%, $H_2O_{t,f}$ = 1.87 wt%, T = 600°C, size 1.16×1.31×0.76 mm)								
Bubble 1	14.0	X1	0.08	12	0.27	0.08	1 215	1 215
B1-5 ($H_2O_{t,i}$ = 2.04 wt%, $H_2O_{t,f}$ = 1.92 wt%, T = 575°C, size 1.19×1.61×0.95 mm)								
Bubble 1	16.1	SS	0.14	2	0.29	0.14	2 700	
B1-6 ($H_2O_{t,i}$ = 2.03 wt%, $H_2O_{t,f}$ = 1.81 wt%, T = 551°C, size 2.69×2.43×0.99 mm)								
Bubble 4	21.6	Z1	0.46	4a	0.11	0.11	10 800	6 600
B1-2 ($H_2O_{t,i}$ = 1.97 wt%, $H_2O_{t,f}$ = 1.77 wt%, T = 525°C, size 1.14×1.51×0.99 mm)								
Bubble 1	17.2	Z1	0.30	3	0.19	0.19	26 820	25 620
B1-3 ($H_2O_{t,i}$ = 1.97 wt%, $H_2O_{t,f}$ = 1.49 wt%, T = 500°C, size 1.28–2×1.13×0.83 mm)								
Bubble 9	8.3	Y0	0.18	8	0.20	0.18	176 220	98 520
B2-1 ($H_2O_{t,i}$ = 1.28–1.45 wt%, $H_2O_{t,f}$ = 1.16–1.36 wt%, T = 600°C, size 1.78×1.73×1.41 mm)								
Bubble 3a	3.7	Z0	0.10	3	0.05	0.05	5 760	3 060
B2-C ($H_2O_{t,i}$ = 1.41 wt%, $H_2O_{t,f}$ = 1.31 wt%, T = 575°C, size 0.86×0.90×1.64 mm)								
Bubble 3	2.5	Y1	0.22	5	0.22	0.22	16 800	
B3-1 ($H_2O_{t,i}$ = 1.44–1.49 wt%, $H_2O_{t,f}$ = 1.39–1.43 wt%, T = 600°C, size 2.67×0.65–1.57×2.33 mm)								
Bubble 3	3.3	Z0	0.14	4	0.50	0.14	3 900	

The complete bubble growth data can be found in table A1 (**EPSL online Background dataset**[1]).
[a]X0 is surface at $X = 0$ and X1 is that at maximum X; similar for Y0 and Y1, and Z0 and Z1. SS indicates slant surface.
[b]The distances to closest surface or closest bubble are calculated from the center of the bubble.
[c]Time when bubble growth is interfered with by a nearby surface/bubble or when the bubble cannot be focussed well.

$H_2O_{t,i}$, and ~0.007 μm/s at 600°C and 1.45 wt% $H_2O_{t,i}$.

In the quantitative discussion on bubble growth rates below, we concentrate on unaffected bubbles (including those with a nearby surface or bubble but t is smaller than the time when this effect becomes noticeable, see t_d given in Table 1). Growth data for bubbles affected by a surface or other bubbles are of comparable quality but cannot be modeled quantitatively at this time. These data may be useful for verifying future models that treat such interactions, and are included and indicated in table A1 (**EPSL Online Background Dataset**[1]).

4. Comparison with bubble growth models

Experimental bubble growth data can be used to verify bubble growth models. Several groups of authors have developed numerical models for bubble growth and each approach is improving. In our opinion, the model of Proussevitch and Sahagian [13] (PS98 hereafter), which is an improvement of the earlier model of Proussevitch et al. [11], is most realistic because it considers bubble growth in a multi-bubble system that is affected by mass transport and viscous flow, and it accounts for the dependence of viscosity and H_2O diffusivity on H_2O content. Other dynamic models [3,5,8–12] are not used because of the approximations in these models (such as constant diffusivity and viscosity). Navon et al. [5] applied a simple analytical solution to treat the initial stage of bubble growth (viscosity-controlled bubble growth with rapid diffusion) [2]. Therefore, we compare experimental bubble growth data with the PS98 model and the analytical solution of [5].

For clarity of the following discussion, the bubble growth model of PS98 [13] is summarized here. The governing equations for isothermal bubble growth include:

1. H_2O diffusion equation (using spherical coordinates):

$$\frac{\partial w}{\partial t} = \frac{1}{r^2}\frac{\partial}{\partial r}\left(Dr^2\frac{\partial w}{\partial r}\right) - v\frac{a^2}{r^2}\frac{\partial w}{\partial r},$$

$$t > 0, \text{ and } a \le r \le S \qquad (1)$$

where w is the concentration (mass fraction) of H_2O_t, t is time, r is the radial coordinate, D is H_2O_t diffusivity that depends on w, v is the bubble growth rate da/dt, a is the bubble radius, and the melt shell region is from $r=a$ to $r=S$ (both a and S increase with time).

2. Hydrodynamics of melt surrounding the bubble:

$$P_g - P_f = \frac{2\sigma}{a} - 4va^2 \int_{z(a)}^{z(S)} \eta(z)\,dz \quad (2)$$

where P_g is the gas pressure in the bubble, P_f is the ambient pressure, σ is the surface tension, $z(a)=1/a^3$, and η is the melt viscosity that depends on H_2O_t content. The integration above accounts for the effect of variable viscosity. For constant viscosity, the above equation reduces to: $P_g - P_f = 2\sigma/a - 4va^2\eta(1/S^3 - 1/a^3) \rightarrow (2\sigma + 4\eta v)/a \rightarrow 4\eta v/a$, where the first arrow applies for infinite S (bubble growth in infinite melt), and the second arrow applies for large bubbles ($a \geq 3$ μm for our experiments) for which surface tension can be ignored. Hence if viscosity controls bubble growth, and if $P_g - P_f$ is roughly constant, bubble growth rate v is roughly $a(P_g - P_f)/(4\eta)$ and proportional to bubble radius a. Because diffusion also plays a main role in bubble growth, our data show that bubble growth rate only increases slightly with bubble radius.

3. Initial conditions: The initial H_2O_t concentration profile adjacent to a bubble is assumed to be uniform. The initial bubble pressure must be specified (see below).

4. Boundary conditions include: (a) mass balance at the bubble–melt interface:

$$\frac{d}{dt}\left(\frac{4}{3}\pi a^3 \frac{\omega P_g}{RT}\right) = 4\pi a^2 D\rho \left(\frac{\partial w}{\partial r}\right)_{r=a} \quad (3)$$

where ω is the molar mass of H_2O, R is the gas constant, and ρ is the density of the melt; (b) interface equilibrium between the melt and gas phases, which dictates that H_2O_t concentration at the interface melt to be the solubility corresponding to pressure of P_g; and (c) symmetry at the outer wall of the melt shell ($r=S$):

$$\left(\frac{\partial w}{\partial r}\right)_{r=S} = 0 \quad (4)$$

The above set of equations can be solved numerically given input parameters.

4.1. Comparison of our bubble growth data with the PS98 model

To solve the above set of equations for isothermal bubble growth, we modified a copy of the PS98 program provided by Proussevitch. For the initial pressure in the bubble, we tried either the ambient pressure 0.1 MPa, or the saturation pressure (at 550°C and 2.03 wt% $H_2O_{t,i}$, the saturation pressure is 14.7 MPa). The difference in the calculated bubble radius is less than 10% relative (Fig. 3a). Because the difference is small and because the shape of the calculated curve with initial pressure of 0.1 MPa matches the data slightly better, we use 0.1 MPa as the initial bubble pressure unless otherwise specified (as in Fig. 5). The actual initial bubble pressure is likely between 0.1 MPa and the saturation pressure, and the initial concentration profile may be nonuniform. Hence, these are two of the uncertainties in modeling experimental bubble growth data. We do not expect the uncertainties to have a major effect on the calculated results.

A constant melt density of 2300 kg/m^3 is used and variation of this parameter by a few percent [25] does not change the results. Surface tension is assumed to be 0.33 N/m [26] and variation of this parameter by a factor of 2 does not significantly change the results. The melt thickness is assumed to be the same as the distance between the wall of a bubble and that of its closest bubble. This distance is not halved because our data show that a single bubble does not significantly affect the growth rate of a neighboring bubble. Furthermore, because we only consider growth of unaffected bubbles, the assumed initial shell thickness does not change the results significantly.

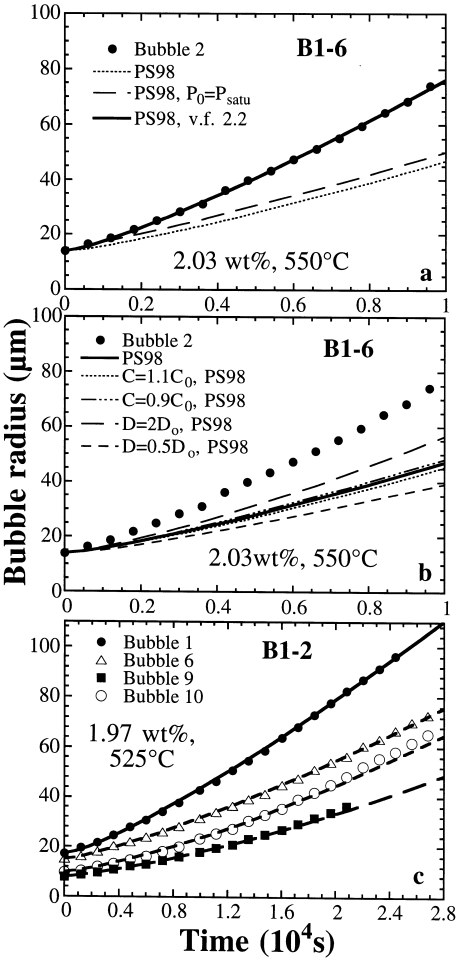

Fig. 3. (a) Comparison of experimental bubble growth data (bubble 2 in experiment B1-6, shown as filled circles) with models. The curves are calculated using the model of PS98. The dotted curve is calculated using the viscosity model of Hess and Dingwell [14], the solid curve is calculated using the viscosity values divided by 2.2, and the long-dashed curve is calculated by assuming initial gas pressure in the bubble equals the saturation pressure. All other parameters are from the literature as discussed in the text. (b) The effect of solubility/diffusivity uncertainties on calculated curves. D is diffusivity and D_0 is calculated using Eq. 5. C is solubility and C_0 is the solubility calculated using Eq. 6. (c) Comparison of experimental bubble growth data for several bubbles in experiment B1-2 with PS98 using the viscosity of [14] divided by a factor (Table 2, Fig. 4).

The most critical input parameters for calculating bubble growth are melt viscosity, H_2O diffusivity and solubility. For total H_2O diffusivity, we use the expression in [27]:

$$D_{H_2O_t} = X\exp(m)\left\{1+\exp\left[56+m+ X\left(-34.1+\frac{44620}{T}+\frac{57.3P}{T}\right)- \sqrt{X}\left(0.091+\frac{4.77\times10^6}{T^2}\right)\right]\right\} \quad (5)$$

where $m=-20.79-5030/T-1.4P/T$, $D_{H_2O_t}$ is in $\mu m^2/s$, X is the mole fraction of H_2O_t on a single oxygen basis, P is in MPa, and T is in K. This model is derived from experimental data covering 0–7.7 wt% H_2O_t, 400–1200°C and 0.1–810 MPa, and can also be applied to model bubble growth data of Lyakhovsky et al. [3] and Gardner et al. [6].

For solubility, we need solubility at relatively low temperature and down to 0.1 MPa pressure, which is a region previous solubility models and data do not cover well. For example, for rhyolitic melt at 850°C, the model of Moore et al. [27] gives a calculated solubility of 0.072 wt%, the formula of Jaupart and Tait [28] gives 0.130 wt%, and Navon et al. [5] adopted 0.10 wt%. Although the absolute difference is small, the relative uncertainty is large and the effect on the resulting bubble growth rate can be large. For an $H_2O_{t,i}$ of 0.14 wt% in Bagdassarov et al. [2], the saturation pressure would be 0.38 MPa using the model of [27], 0.12 MPa using [28], and 0.2 MPa using [5]. The purpose of this discussion is to point out the possible consequences of inaccurate solubility, and is not intended to criticize the models of Moore et al. [27] and Jaupart and Tait [28] because the models were not developed to be accurate at such low pressures. Zhang [16] reviewed solubility data in rhyolitic and quasi-rhyolitic melts [29,30] and formulated the following expression for H_2O_t solubility:

$$X = K_1 f + \frac{K_1 K_2 f(1-K_1 f)}{K_1 K_2 f + \sqrt{(K_1 K_2 f)^2 + 4K_1 K_2 f(1-K_1 f)}} \quad (6)$$

where X is the same as in Eq. 5, f is H_2O fugacity [31], $K_1 = \exp[(-13.869-0.002474P)+(3890.3-3.948P)/T]$, $K_2 = 6.53\exp(-3110/T)$ [15,19,32], P is H_2O vapor pressure in MPa, and T is in K. Its extrapolation to 0.1 MPa at 850°C is in agreement with preliminary data from our laboratory (calculated 0.099% vs. experimental 0.095% [33]). Hence we adopt the solubility model of Zhang [16] in this study.

For viscosity, the model of Hess and Dingwell [14] is used because: (i) it is calibrated by a large data set (including viscosity data covering the temperature and H_2O_t range of our bubble growth experiments); (ii) it accounts for the non-Arrhenian behavior of viscosity versus temperature; and (iii) it is roughly consistent with the independent data set of the apparent equilibrium temperature as a function of cooling rate [34]. The model of Schulze et al. [35] cannot be extrapolated to low temperature because it assumes a simple Arrhenian relation between viscosity and temperature.

When the experimental bubble growth data are compared with the calculated bubble growth curve using PS98, the calculated bubble radii are 10–50% below the experimental radii at 9600 s (e.g., Fig. 3a). The shape of the calculated curve matches that of the experimental growth data. Because there are no free parameters at all, this level of agreement demonstrates that there is consistency between bubble growth data and all other experimental data (among which diffusivity, solubility, and viscosity are the most critical).

We investigate next whether the small differences between our bubble growth data and results of PS98 can be reconciled by changing the input parameters within their specified uncertainties. As already mentioned, changing the initial bubble pressure to the saturation pressure (Fig. 3a), or changing the surface tension by a factor of 2, does not significantly change the calculated results. Changing the solubility by 10% relative (roughly the uncertainty of the model) is not enough to reconcile the data and the calculation (Fig. 3b). Fig. 3b shows that varying the diffusivity by a factor of 2 (greater than the maximum uncertainty of a factor of 1.7) is not enough to reconcile the data and the calculation. The CO_2 effect is difficult to quantify but is estimated to be $\leq 15\%$ based on maximum CO_2/H_2O ratio in the bubbles (**EPSL Online Background Dataset**[1]). Although the combination of all the above factors, when pushed to the extreme, can help significantly in bringing the calculation into agreement with experimental data, the simplest solution to reconcile calculation and experimental data is to reduce the viscosity by a factor (that is, dividing the viscosity from [14] by a factor) that is within the specified uncertainty of a factor of 8 (Fig. 3). The match of not only the values but also the shape of the bubble growth data is extraordinary because there is only one parameter adjusted within its uncertainty.

The correction factor for viscosity for a given series of experiments should be constant for different bubbles. Fig. 4 shows that the correction factor for the viscosity for experiment B1-2 is different for different bubbles, ranging from 2.2 to 4.7. In other samples, the viscosity correction fac-

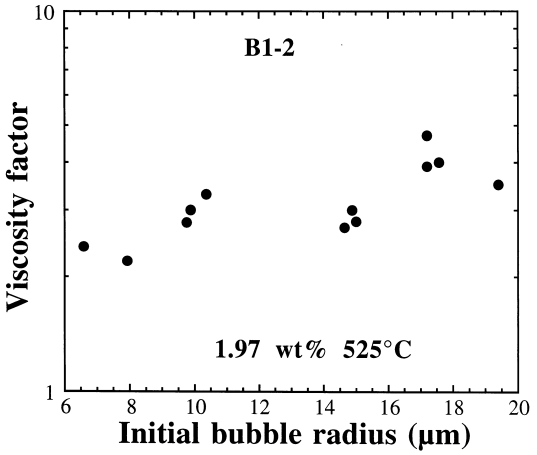

Fig. 4. The viscosity factor inferred for each bubble in experiment B1-2 vs. the initial radius. Most factors fall within 3–4. The scatter is likely caused by the heterogeneity in the initial water concentration.

tor also varies. The most likely explanation of the scatter in the viscosity factor is some local inhomogeneity of $H_2O_{t,i}$ and/or the effect of bubbles and microphenocrysts on magma viscosity. Our numerical simulations indicate that $\leq 15\%$ relative variation of $H_2O_{t,i}$ is enough to explain the scatter in the viscosity factor. In order to verify this, one of the samples (B2-1, 600°C) was measured using a 50 μm aperture for the final H_2O_t close to different bubbles because the sample is still clear enough after the experiments and because bubble growth rates in this sample require the largest range of viscosity factors. The final H_2O_t ranges from 1.16 to 1.36 wt%, roughly corresponding to $H_2O_{t,i}$ of 1.28–1.45 wt% after correction of diffusive water loss from the surfaces. This range of $H_2O_{t,i}$ can account for a factor of 2.2 variation of the viscosity factor. Using the new and variable $H_2O_{t,i}$, the scatter in the viscosity factor decreased significantly (1.8–5 without correction, 1.8–2.3 with correction). Because the heterogeneity is of the scale of a hundred μm but the sample thickness is 1.41 mm, the actual variation in $H_2O_{t,i}$ is likely to be more than we have measured.

If our treatment above is correct, then our bubble growth data provide constraints on effective viscosity. Some viscosity correction factors are listed in Table 2. The grand average of the viscosity correction factor is about 2. Because the viscosity obtained from this work is consistently less than the calculated viscosity using [14] by a factor of about 2, it is possible that the difference is due to the compositional effect although the viscosity model of [14] included some viscosity data for a melt of our rhyolitic composition.

Another way of obtaining viscosity is by fitting the initial stage of our bubble growth data using the simple equation derived by Navon et al. [5]:

$$a = a_{CR} + (a_0 - a_{CR})\exp\left(\frac{P_{dyn}}{4\eta}t\right) \quad (7)$$

where a_0 is the initial radius, $a_{CR} = 2\sigma/(P_s - P_f)$ is the critical radius (P_s is the saturation pressure corresponding to $H_2O_{t,i}$ content) which is negligible compared to a_0, and P_{dyn} is the dynamic pressure that can be found from calculation using PS98 (to improve accuracy, we use P_{dyn} instead of $P_s - P_f$ in [5] because the melt at the bubble–melt interface is slightly depleted in H_2O by bubble growth and because pressure due to surface tension is small). Fitting ln$a$ vs. t for a small t range (corresponding to $\leq 25\%$ variation in calculated P_{dyn} using PS98) by a straight line gives $P_{dyn}/(4\eta)$, from which η can be calculated. Viscosities

Table 2
Selected results from bubble growth modeling

Sample B1-2: 1.97 wt% $H_2O_{t,i}$ at 525°C, $\Delta P = 126$ bar, $\eta_{HD} = 6.18\times10^{10}$ Pa s			
Bubble ID	1	3	9
P_{dyn} (bar)	89–99	93–102	114–119
η (N98)	3.21×10^{10}	3.41×10^{10}	3.56×10^{10}
η (PS98)	1.32×10^{10}	1.59×10^{10}	2.81×10^{10}
v.f. (PS98)	4.7	3.9	2.2
Sample B1-6: 2.03 wt% $H_2O_{t,i}$ at 551°C, $\Delta P = 146$ bar, $\eta_{HD} = 1.35\times10^{10}$ Pa s			
Bubble ID	1	2	7
P_{dyn} (bar)	96–120	98–112	86–107
η (N98)	1.24×10^{10}	1.53×10^{10}	0.10×10^{10}
η (PS98)	0.52×10^{10}	0.61×10^{10}	0.33×10^{10}
v.f. (PS98)	2.6	2.2	4.1
Sample B1-5: 2.04 wt% $H_2O_{t,i}$ at 575°C, $\Delta P = 160$ bar, $\eta_{HD} = 4.16\times10^{9}$ Pa s			
Bubble ID	1	2	6
P_{dyn} (bar)	92–105	88–99	73–81
η (N98)	7.18×10^{9}	7.95×10^{9}	9.18×10^{9}
η (PS98)	1.98×10^{9}	1.81×10^{9}	1.54×10^{9}
v.f. (PS98)	2.1	2.3	2.7
Sample B2-C: 1.41 wt% $H_2O_{t,i}$ at 575°C, $\Delta P = 86$ bar, $\eta_{HD} = 2.77\times10^{10}$ Pa s			
Bubble ID	3	4	5
P_{dyn} (bar)	82–86	84–86	80–85
η (N98)	2.20×10^{10}	2.70×10^{10}	1.90×10^{10}
η (PS98)	1.98×10^{10}	2.52×10^{10}	1.85×10^{10}
v.f. (PS98)	1.4	1.1	1.5
Sample B2-1: 600°C; for 1.28 wt% $H_2O_{t,i}$, $\Delta P = 79$ bar, $\eta_{HD} = 1.34\times10^{10}$ Pa s for 1.45 wt% $H_2O_{t,i}$, $\Delta P = 98$ bar, $\eta_{HD} = 7.41\times10^{9}$ Pa s			
Bubble ID	1	2	6
$H_2O_{t,i}$	1.28 wt%	1.28 wt%	1.45 wt%
P_{dyn} (bar)	77–78	72–75	79–91
η (N98)	0.67×10^{10}	0.61×10^{10}	0.52×10^{10}
η (PS98)	0.67×10^{10}	0.61×10^{10}	0.39×10^{10}
v.f. (PS98)	2	2.2	1.9

ΔP is oversaturation pressure calculated using Eq. 6. Viscosity (η) is calculated at the initial water content and is in Pa s. η_{HD} is calculated using the model of Hess and Dingwell [14]. P_{dyn} range given is calculated from the model of PS98 and is the range to apply Eq. 7 to obtain η (N98) [5]. η (PS98) and v.f. (PS98) are obtained from the model of PS98 so that calculated bubble growth curve matches data.

obtained from different bubbles in a given sample show less scatter than those obtained using PS98 and are in slightly better agreement with those of Hess and Dingwell [14] (Table 2).

We conclude that bubble growth data in this study, the diffusivity model [18], the solubility model [16], and the viscosity model [14] are roughly consistent with each other under the numerical model of Proussevitch and Sahagian [13]. We also conclude that the simple method of Navon et al. [5] for treating the initial growth of bubbles is very useful in deriving viscosity. Our

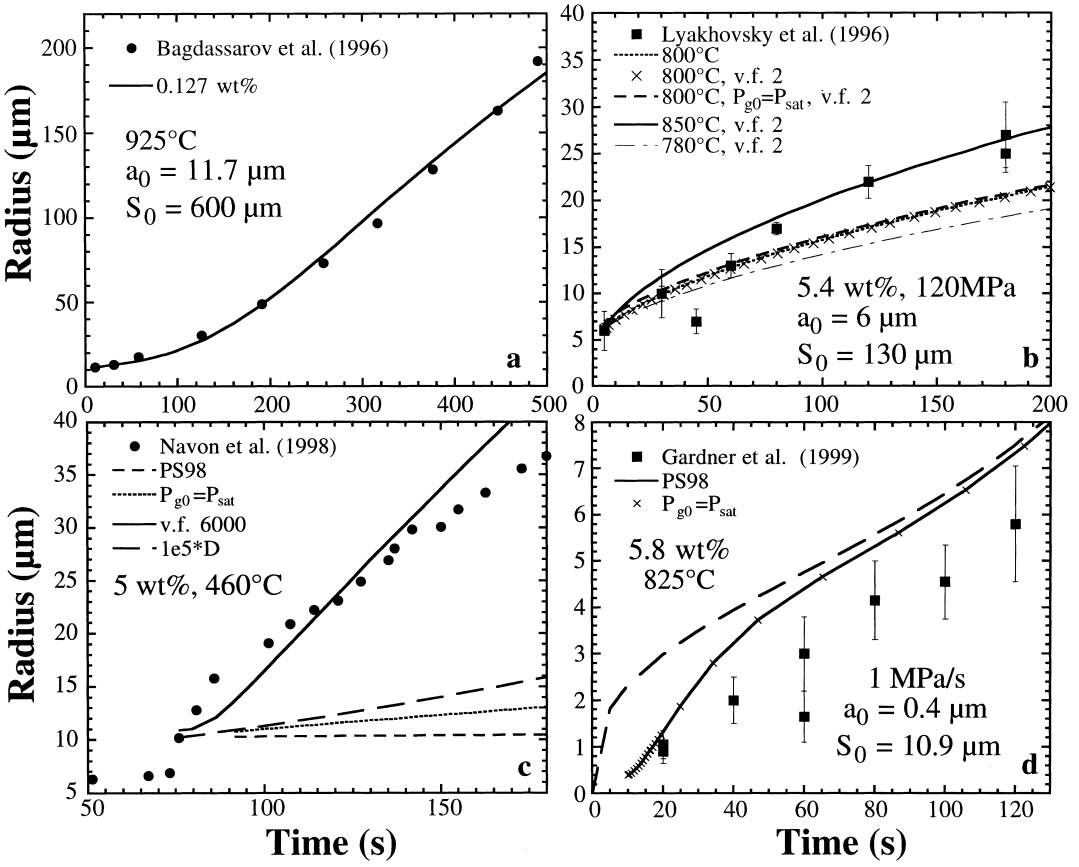

Fig. 5. Comparison of calculated results using PS98 with experimental bubble growth data reported in the literature. Surface tension for all calculations is 0.33 N/m. Solubility is from [16]. Viscosity is from [14] divided by 2 and diffusivity is from [18] except for (a). (a) Data of Bagdassarov et al. [2] (solid circles as read from their paper because the authors did not send data upon request). D for this peralkaline rhyolite is obtained by multiplying D in calc-alkaline rhyolite [18] by 3.3, based on the data of [37]. Viscosity is from [2]. Solid line: $H_2O_{t,i}$ is 0.127 wt% and S_0 is 600 μm. (b) Data of Lyakhovsky et al. [3] (solid squares). The experimental data are bracketed by calculations at 780 and 850°C. Bubble growth is largely controlled by diffusion (note the parabolic shape of the curve) and the effect of viscosity is small. (c) Data from Navon et al. [5] (solid circles). Because the temperature was increasing during the initial stage, we started the calculation at a bubble size of 10 μm when the experimental temperature reached 460°C. $S_0 = 250$ μm. Medium-dashed line is calculated using PS98 and the solubility expression in [5]: $C = 4.33 \times 10^{-6} P^{1/2}$ where P is in Pa. Solid line is calculated using PS98 and solubility model in [16] and by modifying the viscosity by a factor of 6000. Increasing diffusivity by five orders of magnitude (long-dashed line) is not enough to bring the data and calculation into agreement. (d) Decompression (1 MPa/s) experimental data of Gardner et al. [6] (squares). The samples are hydrated at 200 MPa and then decompressed, and we use extrapolated bubble radius at 190 MPa [6] as the initial bubble radius (0.4 μm). Initial S (melt shell thickness plus bubble radius) is calculated from $4\pi N(S^3 - a^3)/3 = 1$ to be 10.9 μm where N is the average number density of decompression bubbles per unit volume of bubble-free melt. The solid line is calculated from the dynamic bubble growth model of PS98 and the long-dashed curve is for equilibrium bubble growth upon decompression.

results constitute the first experimental verification of a bubble growth model. Bagdassarov et al. [2] compared experimental data with numerical calculations, which is close to an experimental verification although the details of the bubble growth program are not given. Navon et al. [5] also tried to verify their bubble growth model with their data but they made viscosity and diffusivity fitting parameters. Furthermore, the bubble growth model of Navon et al. [5] did not consider the expected large variation of $D_{H_2O_t}$ over an H_2O_t range of 0.1–5 wt% [36]. Hence, we suggest that the results of Navon et al. [5] are best described as a fit instead of a verification of a bubble growth model. As will be seen next, their bubble growth data are in fact the only data that cannot be reconciled with calculation at this time.

4.2. Comparison of other bubble growth data with the PS98 model

We also compared bubble growth data in the literature with the results of PS98 (Fig. 5). Fig. 5a shows a example of comparison of data of Bagdassarov et al. [2] with the calculation, and good agreement is obtained by varying the $H_2O_{t,i}$ within its uncertainty. Fig. 5b shows a comparison of data of Lyakhovsky et al. [3] at 780–850°C and 120 MPa (initial hydration pressure at 150 MPa) with calculation of PS98. The calculated growth curve at 780°C and that at 850°C roughly bracket the range of bubble growth data, demonstrating excellent agreement between calculation and experimental data. Fig. 5c shows a comparison of bubble growth data of Navon et al. [5] at 460°C and 0.1 MPa with high $H_2O_{t,i}$ (5 wt%), which Navon et al. [5] used to verify their own bubble growth model. The calculation is inconsistent with the data unless we decrease the viscosity by a factor of 6000 (Fig. 5c), much outside the model uncertainty specified by the original authors [14].

All the above bubble growth data are for isobaric bubble growth. Fig. 5d compares bubble growth data under constant-rate decompression of 1 MPa/s by Gardner et al. [6] with PS98. The calculated curve is on average 30% above the experimental results (Fig. 5d). Similar differences are observed when 0.25 MPa/s data and calculation are compared. Because there are no free parameters, this degree of agreement is very good. Furthermore, the decompressional bubble growth data suffer from an experimental problem of hydration bubbles. The slightly slow growth rate in the experiments probably reflects a combination of: (i) the effect of hydration bubbles in reducing H_2O in the melt and/or (ii) uncertainty in estimating bubble number density and bubble size. Hence we concur with Navon et al. [5] that the experimentally verified bubble growth model using isobaric bubble growth data can be safely extended to simulate bubble growth under conditions of variable pressure.

To summarize, most recent bubble growth data (this study, [2,3,6]) can be calculated using the PS98 model with assessed diffusivity and solubility and with viscosity adjusted within its uncertainty. The only exception is the data of Navon et al. [5], probably due to uncertainties in viscosity and diffusivity (there are no experimental viscosity nor diffusivity data at the P–T–X conditions of the experiments), or experimental problems. We conclude that bubble growth as a function of time can be calculated for rhyolitic melt as long as appropriate expressions of diffusivity, solubility and viscosity are used.

5. Conclusions

1. We report detailed experimental data on bubble growth at atmospheric pressure for natural rhyolitic melts with 1.3–2.0 wt% $H_2O_{t,i}$. Our data, recent solubility/diffusivity/viscosity models, and the bubble growth model of Proussevitch and Sahagian [13] are consistent with each other within uncertainty.
2. Other experimental bubble growth data in rhyolitic melt, including bubble growth data under constant-rate decompression, can be calculated using the verified bubble growth model and appropriate diffusivity and viscosity, except for a T–P–X region of low pressure (0.1 MPa), ≤ 500°C, and $H_2O_{t,i} > 4$ wt%.
3. With a verified bubble growth model, systematic investigation of viscosity and H_2O diffusiv-

ity as a function of H_2O content in dacitic, andesitic, and basaltic melts, and for peralkaline melts is necessary for predicting bubble growth rates in these melts.

Acknowledgements

We thank Wenbing Yu and Jungsan Sohn for participating in the early stage of this research, R.S.J. Sparks, J.E. Gardner, and D. Dingwell for their careful and insightful reviews, R.A. Lange for informal comments, A.A. Proussevitch for providing the source code of the PS98 bubble growth model, O. Navon for providing his reading of bubble growth data from a figure of Bagdassarov et al., and Zhengjiu Xu and Jim Windak for help with FTIR. This work is supported by NSF Grants EAR-9458368, EAR-9706107, EAR-9725566, and EAR-9972937.*[FA]*

References

[1] T. Murase, A.R. McBirney, Properties of some common igneous rocks and their melts at high temperatures, Geol. Soc. Am. Bull. 84 (1973) 3563–3592.
[2] N.S. Bagdassarov, D.B. Dingwell, M.C. Wilding, Rhyolite magma degassing: an experimental study of melt vesiculation, Bull. Volcanol. 57 (1996) 587–601.
[3] V. Lyakhovsky, S. Hurwitz, O. Navon, Bubble growth in rhyolitic melt: experimental and numerical investigation, Bull. Volcanol. 58 (1996) 19–32.
[4] S. Hurwitz, O. Navon, Bubble nucleation in rhyolitic melts: experiments at high pressure, temperature, and water content, Earth Planet. Sci. Lett. 122 (1994) 267–280.
[5] O. Navon, A. Chekhmir, V. Lyakhovsky, Bubble growth in highly viscous melts: theory, experiments, and autoexplosivity of dome lavas, Earth Planet. Sci. Lett. 160 (1998) 763–776.
[6] J.E. Gardner, M. Hilton, M.R. Carroll, Experimental constraints on degassing of magma: isothermal bubble growth during continuous decompression from high pressure, Earth Planet. Sci. Lett. 168 (1999) 201–218.
[7] P.S. Epstein, M.S. Plesset, On the stability of gas bubbles in liquid-gas solutions, J. Chem. Phys. 18 (1950) 1505–1509.
[8] R.S.J. Sparks, The dynamics of bubble formation and growth in magmas: a review and analysis, J. Volcanol. Geotherm. Res. 3 (1978) 1–37.
[9] A. Toramaru, Vesiculation process and bubble size distributions in ascending magmas with constant velocities, J. Geophys. Res. 94 (1989) 17523–17542.
[10] A. Toramaru, Numerical study of nucleation and growth of bubbles in viscous magmas, J. Geophys. Res. 100 (1995) 1913–1931.
[11] A.A. Proussevitch, D.L. Sahagian, A.T. Anderson, Dynamics of diffusive bubble growth in magmas: isothermal case, J. Geophys. Res. 98 (1993) 22283–22307.
[12] A.A. Proussevitch, D.L. Sahagian, Dynamic of coupled diffusive and decompressive bubble growth in magmatic systems, J. Geophys. Res. 101 (1996) 17447–17455.
[13] A.A. Proussevitch, D.L. Sahagian, Dynamics and energetics of bubble growth in magmas: analytical formulation and numerical modeling, J. Geophys. Res. 103 (1998) 18223–18251.
[14] K.-U. Hess, D.B. Dingwell, Viscosities of hydrous leucogranitic melts: a non-Arrhenian model, Am. Miner. 81 (1996) 1297–1300.
[15] Y. Zhang, E. Stolper, G. Wasserburg, Diffusion of water in rhyolitic glasses, Geochim. Cosmochim. Acta 55 (1991) 441–456.
[16] Y. Zhang, H_2O in rhyolitic glasses and melts: measurement, speciation, solubility, and diffusion, Rev. Geophys. 37 (1999) 493–516.
[17] E.B. Watson, Diffusion in volatile-bearing magmas, Rev. Mineral. 30 (1994) 371–411.
[18] Y. Zhang, H. Behrens, H_2O diffusion in rhyolitic melts and glasses, Chem. Geol. (2000) (in press).
[19] Y. Zhang, R. Belcher, P.D. Ihinger, L. Wang, Z. Xu, S. Newman, New calibration of infrared measurement of dissolved water in rhyolitic glasses, Geochim. Cosmochim. Acta 61 (1997) 3089–3100.
[20] F. Fine, E.M. Stolper, The speciation of carbon dioxide in sodium aluminosilicate glasses, Contrib. Mineral. Petrol. 91 (1985) 105–121.
[21] K. Sieh, M. Bursik, Most recent eruptions of the Mono Craters, eastern central California, J. Geophys. Res. 91 (1986) 12539–12571.
[22] S. Newman, S. Epstein, E.M. Stolper, Water, carbon dioxide, and hydrogen isotopes in glasses from the ca. 1340 A.D. eruption of the Mono Craters, California: Constraints on degassing phenomena and initial volatile content, J. Volcanol. Geotherm. Res. 35 (1988) 75–96.
[23] Y. Zhang, Mechnical and phase equilibria in inclusion-host systems, Earth Planet. Sci. Lett. 157 (1998) 209–222.
[24] J.G. Blank, E.M. Stolper, M.R. Carroll, Solubilities of carbon dioxide and water in rhyolitic melt at 850°C and 750 bars, Earth Planet. Sci. Lett. 119 (1993) 27–36.
[25] F.A. Ochs, R.A. Lange, The partial molar volume, thermal expansivity, and compressibility of H_2O in $NaAlSi_3O_8$ liquid: new measurements and an internally consistent model, Contrib. Mineral. Petrol. 129 (1997) 155–165.
[26] D. Walker, O. Mullins Jr., Surface tension of natural silicate melts from 1,200°–1,500°C and implications for

melt structure, Contrib. Mineral. Petrol. 76 (1981) 455–462.

[27] G. Moore, T. Vennemann, I.S.E. Carmichael, An empirical model for the solubility of H_2O in magma to 3 kilobars, Am. Miner. 83 (1998) 36–42.

[28] C. Jaupart, S. Tait, Dynamics of eruptive phenomena, in: J. Nicholls and J.K. Russell (Eds.), Modern Methods of Igneous Petrology: Understanding Magmatic Processes, Reviews in Mineralogy 24, Mineralogical Society of America, Washington, DC, 1990, pp. 213–238.

[29] F. Holtz, H. Behrens, D.B. Dingwell, R.P. Taylor, Water solubility in aluminosilicate melts of haplogranite composition at 2 kbar, Chem. Geol. 96 (1992) 289–302.

[30] F. Holtz, H. Behrens, D.B. Dingwell, W. Johannes, H_2O solubility in haplogranitic melts: compositional, pressure, and temperature dependence, Am. Miner. 80 (1995) 94–108.

[31] K.S. Pitzer, S.M. Sterner, Equations of state valid continuously from zero to extreme pressures for H_2O and CO_2, J. Chem. Phys. 101 (1994) 3111–3116.

[32] P.D. Ihinger, Y. Zhang, E.M. Stolper, The speciation of dissolved water in rhyolitic melts, Geochim. Cosmochim. Acta 63 (1999) 3567–3578.

[33] Y. Liu, Y. Zhang, H_2O solubility in natural rhyolitic melts at 1 bar pressure: preliminary results, EOS Trans. AGU 80 (1999) S350.

[34] Y. Zhang, J. Jenkins, Z. Xu, Kinetics of the reaction $H_2O+O \Leftrightarrow 2OH$ in rhyolitic glasses upon cooling: geospeedometry and comparison with glass transition, Geochim. Cosmochim. Acta 61 (1997) 2167–2173.

[35] F. Schulze, H. Behrens, F. Holtz, J. Roux, W. Johannes, The influence of H_2O on the viscosity of a haplogranitic melt, Am. Miner. 81 (1996) 1155–1165.

[36] M. Nowak, H. Behrens, An experimental investigation on diffusion of water in haplogranitic melts, Contrib. Mineral. Petrol. 126 (1997) 365–376.

[37] Y. Zhang, H. Behrens, H_2O diffusion in silicate glasses and melts, Mineral. Mag. 62A (1998) 1695–1696.